

TOWARDS SMOOTH VIDEO COMPOSITION

Qihang Zhang¹ Ceyuan Yang² Yujun Shen³ Yinghao Xu¹ Bolei Zhou⁴

¹The Chinese University of Hong Kong, ²Shanghai AI Laboratory, ³Ant Group,

⁴University of California, Los Angeles

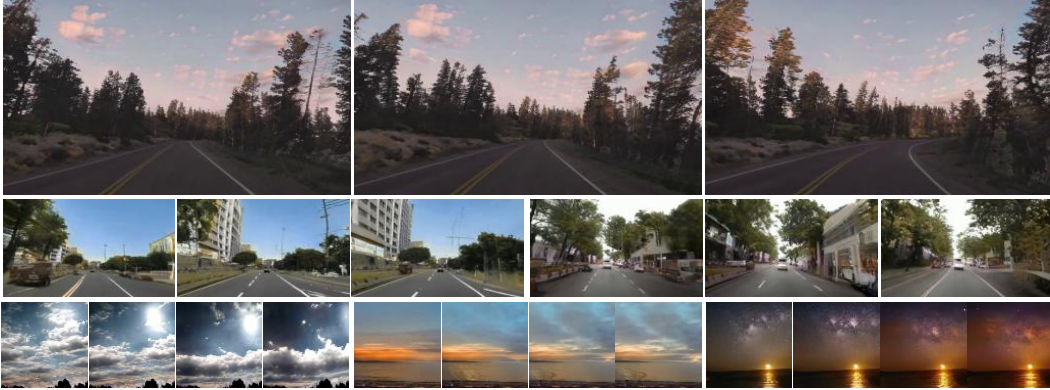


Figure 1: Generated video frames from the proposed model trained on Countryside, YouTube Driving (Zhang et al., 2022), and SkyTimelapse (Xiong et al., 2018) (from top to bottom).

ABSTRACT

Video generation requires synthesizing consistent and persistent frames with dynamic content over time. This work investigates modeling the temporal relations for composing video with arbitrary length, from a few frames to even infinite, using generative adversarial networks (GANs). First, towards composing adjacent frames, we show that the alias-free operation for single image generation, together with adequately pre-learned knowledge, brings a smooth frame transition without compromising the per-frame quality. Second, by incorporating the temporal shift module (TSM), originally designed for video understanding, into the discriminator, we manage to advance the generator in synthesizing more consistent dynamics. Third, we develop a novel B-Spline based motion representation to ensure temporal smoothness to achieve infinite-length video generation. It can go beyond the frame number used in training. A low-rank temporal modulation is also proposed to alleviate repeating contents for long video generation. We evaluate our approach on various datasets and show substantial improvements over video generation baselines. Code and models will be publicly available at <https://genforce.github.io/StyleSV>.

1 INTRODUCTION

Synthesizing images using generative adversarial network (GAN) (Goodfellow et al., 2014; Radford et al., 2016; Karras et al., 2019; 2020b; 2021; 2018) usually requires composing diverse visual concepts and their spatial arrangement. Recent advances in GANs have enabled many appealing applications such as customized editing (Goetschalckx et al., 2019; Shen et al., 2020; Jahanian et al., 2020; Yang et al., 2021) and animation (Qiu et al., 2022; Alaluf et al., 2022). However, employing GANs for video generation remains challenging given the additional requirement of modeling the temporal dynamics.

In fact, a video is not simply a stack of images. Instead, the content in video frames should have a smooth transition over time, and the video may last arbitrarily long. Thus, compared to image synthesis, the crux of video synthesis lies in modeling the temporal relations across frames. We

categorize the temporal relations into three folds regarding the time scale. First, when looking at a transient dynamic, we focus more on the subtle change between neighbor frames and expect decent local motions, such as facial muscle movement and cloud drifting. When the duration becomes longer, more content may vary across frames. Under such a case, it is vital to learn a consistent global motion representation. For example, in a first-view driving video, trees and buildings on the sides of the road should move backward when the car is driving forward. Finally, in videos that last longer, new objects have to be generated over time. Therefore it requires the movements of the newly added objects are consistent and coherent.

This work aims at smooth video composition by modeling multi-scale temporal relations with GANs. First, we confirm that, same as in image synthesis, the texture sticking problem (*i.e.*, some visual concepts are bound to their coordinates) also exists in video generation, interrupting the smooth flow of content across frames. To tackle this issue, we deploy the alias-free technique (Karras et al., 2021) from single image generation and preserve the frame quality via appropriate pre-training. Then, to make the generator produce realistic motion dynamics, we incorporate a temporal shift module (TSM) (Lin et al., 2019) in the discriminator as an inductive bias. Thus the discriminator captures more information from the temporal dimension for real/fake classification, providing better guidance to the generator. Furthermore, we observe that the motion representation proposed in previous work (Skorokhodov et al., 2022) suffers from undesired content jittering (see Sec. 2.4 for details) for long video generation. We identify its cause as the first-order discontinuity when interpolating motion embeddings. To mitigate this issue, we design a novel B-Spline based motion representation that can transit smoothly over time. A low-rank strategy is further proposed to alleviate the issue that the content across frames may repeat cyclically. We evaluate the improved models on various video generation benchmarks, including YouTube driving dataset (Zhang et al., 2022), SkyTimelapse (Xiong et al., 2018), Taichi-HD (Siarohin et al., 2019b) and observe consistent and substantial improvements over existing alternatives. Given its simplicity and efficiency, our approach brings a simple yet strong baseline for video generation.

2 METHOD

We introduce several improvements made on the prior art StyleGAN-V (Skorokhodov et al., 2022) to set a new baseline for video generation. We first introduce the default configuration (**Config-A**) of the StyleGAN-V in Sec. 2.1. We then make a comprehensive overhaul of it. Concretely, in Sec. 2.2 we confirm that the alias-free technique (**Config-B**) in single image generation, together with adequately pre-learned knowledge (**Config-C**), results in a smooth transition of two adjacent frames. Sec. 2.3 shows that when the temporal information is explicitly modeled into the discriminator through the temporal shift module (Lin et al., 2019) (**Config-D**), the generator produces significantly better dynamic content across frames. Although prior arts could already generate arbitrarily long videos, the cyclic jittering is observed as a video continues. Thus We propose a B-Spline based motion representation (**Config-E**) to ensure the continuity, which together with a low-rank temporal modulation (**Config-F**) produces much more realistic long videos in Sec. 2.4.

2.1 PRELIMINARY

StyleGAN-V (Skorokhodov et al., 2022) introduces continuous motion representations and a holistic discriminator for video generation. Specifically, continuous frames I_t could be obtained by feeding continuous t into a generator $G(\cdot)$:

$$I_t = G(u, v_t), \quad (1)$$

where u and v_t denote the content code and continuous motion representation. Concretely, content code is sampled from a standard distribution while the motion representation v_t consists of two embeddings: time positional embedding v_t^{pe} and interpolated motion embedding v_t^{me} .

To obtain the time positional embedding v_t^{pe} , we first randomly sample N_A codes as a set of discrete time anchors $A_i, i \in [0, \dots, N_A - 1]$ that share equal interval (256 frames in practice). Convolutional operation with 1D kernel is then applied on anchor A_i for temporal modeling, producing the corresponding features a_i with timestamp t_i . For an arbitrary continuous t , its corresponding interval is first found with the nearest left and right anchor feature a_l and a_{l+1} , at time t_l and t_{l+1} , so that $t_l \leq t < t_{l+1}, l \in [0, \dots, N_A - 2]$. For time positional embedding v_t^{pe} ,

Table 1: **Evaluation of various configurations.** **Config-A** is the baseline model StyleGAN-V (Skorokhodov et al., 2022). **Config-B** and **Config-C** target fixing the texture sticking issue yet maintain the per-frame quality (Sec. 2.2), which is primarily evaluated by FID. **Config-D** aims to help the generator to produce more reasonable dynamics (Sec. 2.3), which is primarily evaluated by FVD₁₆ and FVD₁₂₈. **Config-E** and **Config-F** alleviate the discontinuity when interpolating motion embeddings (Sec. 2.4). For all metrics, a lower number is better.

| Configuration | SkyTimelapse | | | YouTube Driving | | | Taichi-HD | | |
|--------------------|--------------|-------------------|--------------------|-----------------|-------------------|--------------------|-------------|-------------------|--------------------|
| | FID | FVD ₁₆ | FVD ₁₂₈ | FID | FVD ₁₆ | FVD ₁₂₈ | FID | FVD ₁₆ | FVD ₁₂₈ |
| A StyleGAN-V | 40.8 | 73.9 | 248.3 | 28.3 | 449.8 | 460.6 | 33.8 | 152.0 | 267.3 |
| B + Alias free | 54.0 | 118.8 | 221.4 | 56.4 | 729.8 | 886.0 | 31.4 | 171.7 | 522.9 |
| C + Image pretrain | 52.2 | 73.5 | 230.3 | 15.6 | 272.8 | 447.5 | 20.8 | 104.3 | 314.2 |
| D + TSM | 49.9 | 49.0 | 135.9 | 19.2 | 207.2 | 221.5 | 26.0 | 84.6 | 176.2 |
| E + B-Spline | 63.5 | 64.8 | 185.3 | 21.8 | 281.6 | 375.2 | 25.5 | 82.6 | 169.7 |
| F + Low-rank | 60.4 | 61.9 | 229.1 | 23.0 | 260.4 | 278.9 | 24.8 | 98.3 | 186.8 |

a wave function is derived with learned frequency β , phase γ and amplitude α from the left anchor feature a_l :

$$\begin{aligned} \alpha &= M_\alpha(a_l), \beta = M_\beta(a_l), \gamma = M_\gamma(a_l), \\ v_t^{pe} &= \langle \alpha \cdot \sin(\beta \cdot t + \gamma), \alpha \cdot \cos(\beta \cdot t + \gamma) \rangle, \end{aligned} \quad (2)$$

where $M_\alpha, M_\beta, M_\gamma$ are learnable MLPs. The interpolated motion embedding v_t^{me} could be obtained through linear interpolation between anchor feature a_l and a_{l+1} based on t :

$$v_t^{me} = \frac{(t - t_l)a_l + (t_{l+1} - t)a_{l+1}}{t_{l+1} - t_l}. \quad (3)$$

The final motion representation v_t is thus the sum of these two terms:

$$v_t = v_t^{pe} + v_t^{me}. \quad (4)$$

Additionally, a sparse sampling strategy is proposed for efficient training. Namely, N_t discrete time steps t_i and real video frames I_i are sampled respectively. By feeding N_t discrete time steps and one content code into generator, multiple synthesis $I'_i = G(u, v_{t_i})$ are obtained. In order to distinguish real video frames from synthesized ones, a discriminator $D(\cdot)$ extracts feature y_i for the individual frame, and then a fusion function Θ would perform the temporal aggregation over all frames:

$$y = \Theta(y_i) = \Theta(D(I_i)), \quad i = 0, 1, \dots, N_t - 1. \quad (5)$$

The final discriminative logit l is computed by a MLP M conditioned on time steps:

$$l = M(y, t_0, \dots, t_{N_t-1}). \quad (6)$$

In the following sections, we would make a comprehensive overhaul of the default config, leading to a new simple yet strong approach for video generation.

2.2 ALIAS-FREE OPERATIONS AND PRE-LEARNED KNOWLEDGE

Generated frames within a short temporal window usually share similar visual concepts while the micro motion gradually occurs. Therefore, the smooth transition between frames tends to make the synthesis much more realistic. However, by examining the synthesized frames of StyleGAN-V, we find that texture sticking (Karras et al., 2021) exists. We track the pixels at certain coordinates as the video continues and the *brush effect* in Fig. 2a indicates that these pixels actually move little. Thus, the texture sticks to fixed coordinates.

Alias-free operations (Config-B). To mitigate the texture sticking issue, we follow the StyleGAN3 (Karras et al., 2021) to adopt the alias-free technique in the generator, which reduces the dependency on absolute pixel coordinates. As shown in Fig. 2b, *brush effect* disappears *i.e.*, texture sticking is significantly alleviated by the alias-free technique.

However, as reported in Tab. 1, direct adoption of StyleGAN3 brings lower performance in terms of the FID and FVD scores. One possible reason is that the training receipt is directly inherited

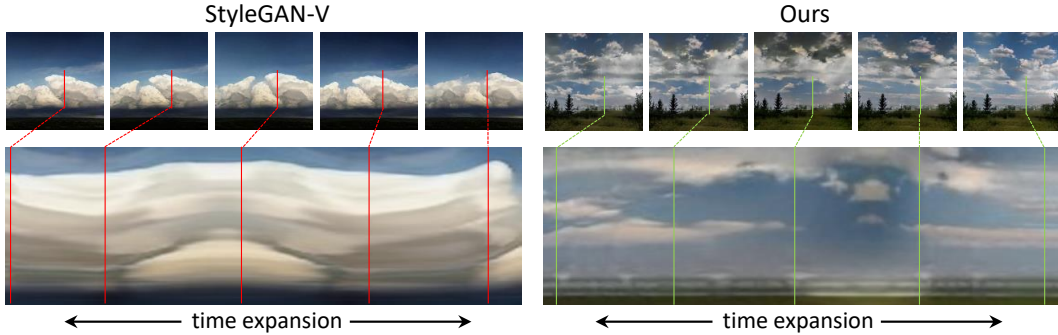


Figure 2: **Visualization of the texture sticking effect.** On the top are a few samples from a continuous sequence of frames, while the bottom visualizes the varying content at a fixed position. We can observe the brush effect from the baseline (Skorokhodov et al., 2022), where the pixel values are strongly anchored to the coordinates. Instead, our approach achieves smoother frame transition between neighbor frames.

from the original StyleGAN-V without any modification. Despite its impairment on FID and FVD to some extent, we still use StyleGAN3 for the sake of its alias-free benefit.

Pre-learned knowledge (Config-C). Simply replacing the generator backbone with StyleGAN3 deteriorates the synthesis. To fix it, we propose to make the best of pre-learned knowledge of image generation network. As discussed before, the key challenge for video generation is to model temporal relations between frames. However, it is entangled with the target of modeling image distribution. We confirm that pre-training at the image level and then fine-tuning at the video level can decouple the two targets of modeling individual frames and cross-frame dynamics. As discovered in (Karras et al., 2019; Yang et al., 2021), GAN’s deep layers mainly control details, for example, coloring, detailed refinements, and etc. We hypothesize that these parts’ knowledge can be pre-learned and re-used in the video generation learning process.

To be specific, we set N_t as 1 in Eq. (5), and train the whole network from scratch as the image pre-training stage. Then deep layers’ weights are loaded in the video fine-tuning stage. With pre-trained deep layers’ weights, now the optimization process can focus on early layers to learn to model sequential changes in structures that show realistic movements. As shown in Tab. 1, after adopting **Config-C**, the generated quality gets improved compared to **Config-B**. Now, with the alias-free technique, we achieve smooth frame transition without compromising the per-frame quality.

2.3 EXPLICIT TEMPORAL REASONING IN DISCRIMINATOR

In the adversarial learning of GAN, it is essential to have a strong discriminator, assuring the sufficient training of the generator. In the video generation task, the discriminator thus has to model the temporal relations of multiple frames to distinguish unnatural movements from real ones. However, in previous work only a simple concatenation operation \oplus is used: $y = \bigoplus_i y_i$, where y_i denotes a single frame’s feature extracted by the discriminator and y denotes the feature after temporal fusion.

Temporal modeling (Config-D). We incorporate an explicit temporal modeling approach *i.e.*, temporal shift module (TSM) that shows exceptional performance for video classification. Concretely, at each convolution layer before temporal fusion, we have features from multiple frames: $y_i^n \in \mathcal{R}^{H \times W \times C}$, $i = 0, \dots, N_t - 1$, where n is the layer index, H and W are the feature map resolution and C is the feature channel number. Then, TSM performs channel-wise swapping between adjacent frames:

$$y_i^n(x, y) \leftarrow \bigoplus_3(y_{i-1}^n(x, y)[\frac{C}{8}], y_i^n(x, y)[\frac{C}{8} : \frac{7C}{8}], y_{i+1}^n(x, y)[\frac{7C}{8} :]), \quad (7)$$

where $\bigoplus_3(\cdot)$ is a concatenation operation, and (x, y) are arbitrary coordinates. In this way, one quarter of the channels of a single frame after temporal fusion contain information from adjacent frames. Follow-up convolution kernels in deeper layers can perform efficient temporal reasoning based on this mixed representation. In our ablation study, while FID becomes slightly worse

StyleGAN-V

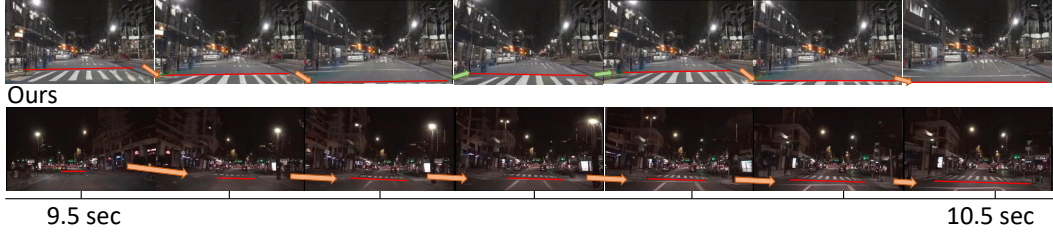


Figure 3: **Visualization of the content jittering effect.** As the video continues, we can observe the unstable crossroad in the baseline model (Skorokhodov et al., 2022), caused by discontinuous motion representation. Instead, our approach alleviates it through the proposed B-Spline motion representation.

compared to **Config-C**, adopting explicit temporal modeling (**Config-D**) improves FVD_{16} and FVD_{128} substantially, yielding over 100% improvement on YouTube Driving dataset.

2.4 TOWARDS INFINITE VIDEO GENERATION

The metrics FID, FVD_{16} and FVD_{128} used before merely measure the synthesis quality of the relatively short videos (e.g., 128 frames usually cover around 6 seconds), we further investigate whether current configuration is able to produce arbitrarily long videos. Note that, by saying arbitrarily long, we mean infinite length along the time axis, not infinite content. Ideally, we could easily generate an infinite number of frames by continuously sampling time t . The generator is supposed to produce the corresponding synthesis. However, as the video continues, a conspicuous jittering effect occurs periodically every 10 seconds. For example, Fig. 3 shows the crossroad moves forward at the beginning, and then suddenly goes backward.

Discontinuity of motion embeddings. As introduced in Sec. 2.1, motion embedding v_t contains time positional embedding v_t^{pe} and interpolated motion embedding v_t^{me} . In particular, v_t^{pe} could be obtained by a learned wave function on the left nearest anchor feature a_l while the motion embedding v_t^{me} derives from the linear interpolation between the left and right anchor feature a_l and a_{l+1} . This interpolation would result in the first-order discontinuity for both learned wave function and linear interpolation when getting through multiple anchors, as shown in Fig. 4a. Moreover, when the T-SNE (Van der Maaten & Hinton, 2008) is applied to the motion embedding given a long period, we can see in Fig. 5a that such discontinuity causes the drastic change and jittering in the generated content.

B-Spline based motion representations (Config-E). With an assumption of the discontinuity of motion embeddings, we design a basic spline (B-Spline) based motion representation that could guarantee first-order numerical smoothness. To be specific, B-Spline of order n is a piece-wise polynomial function of degree $n - 1$ in a given variable. It is widely used in computer-aided design and computer graphics for curve fitting, controlling a smooth curve with calculated weights w_i on several control points. In particular, the number of control points is determined by the order of the B-Spline. With a pre-defined knot sequence $\{t_i\}$, a B-Spline with any order can be defined by means of the Cox-de Boor recursion formula (de Boor, 1971). The first-order B-Spline is then defined by:

$$B_{i,1}(t) := \begin{cases} 1 & \text{if } t_i \leq t < t_{i+1}, \\ 0 & \text{otherwise.} \end{cases} \quad (8)$$

Here i is the interval index. B-spline of higher orders is further defined recursively:

$$B_{i,k+1}(t) := \omega_{i,k}(t)B_{i,k}(t) + [1 - \omega_{i+1,k}(t)]B_{i+1,k}(t), \quad (9)$$

where k is the order and

$$\omega_{i,k}(t) := \begin{cases} \frac{t-t_i}{t_{i+k}-t_i} & t_{i+k} \neq t_i, \\ 0 & \text{otherwise.} \end{cases} \quad (10)$$

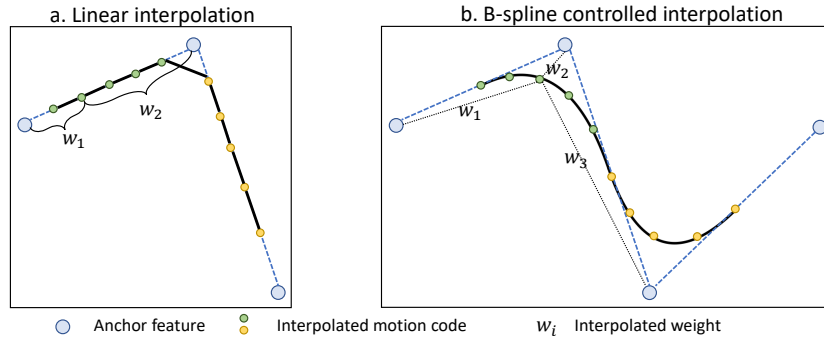


Figure 4: **Comparison between linear interpolation and our B-Spline controlled interpolation.** B-spline is able to smooth the interpolation between various anchor features, and hence improve the first-order numerical continuity.

We treat each anchor feature a_i as the control point and use $B_{i,k}(t)$ as its corresponding weight given time t . Hence, B-Spline based anchor feature is defined as:

$$\hat{a}(t) = \sum_i B_{i,k}(t)a_i. \quad (11)$$

We further use $\hat{a}(t)$ instead of discretized a_i to calculate time positional embedding v_t^{pe} and interpolated motion embedding v_t^{me} as defined in Eq. (2) and Eq. (3). Fig. 4b suggests the continuity property of B-Spline. Meanwhile, through T-SNE again, the B-Spline based motion representations become much smoother in Fig. 5b. As shown in Fig. 3, the crossroad gradually approaches the observer without any sudden jittering.

Low-rank temporal modulation (Config-F). After adopting B-Spline based motion embedding, the jittering effect gets erased. However, we find that similar content periodically appears as video continues (see Fig. A6a). This result implies that motion embedding poorly represents visual concepts. We thus hypothesize that the new motion embedding might be endowed with a stronger capacity to represent various visual concepts. Inspired by recent works (Bau et al., 2020; Wang et al., 2022a), we suppress the representation capacity through the low-rank strategy.

Original StyleGAN-based architecture incorporates styles into convolutional kernels via modulation trick (Karras et al., 2020a). When generating videos, a similar technique is also applied with small modifications. Content embedding u together with the motion embedding v_t would be fed into an affine layer M , generating the style code to modulate the original weight W :

$$W' = W \cdot M(u \oplus v_t), \quad (12)$$

where \oplus stands for the concatenation operation. That is, motion and content embedding could equally contribute to the final style to change the visual concepts of frames. In order to suppress the representational capacity of motion embeddings, we first separate the motion and content codes and then replace the kernel regarding the motion code with a low-rank one:

$$W' = W_{co} \cdot M_{co}(u) + W_{mo} \cdot M_{mo}(v_t), \text{ where } W_{mo} = UV, \quad (13)$$

where U, V is tall matrix that guarantees W_{mo} is a low-rank matrix. With such a low-rank strategy, the capacity of motion embedding is suppressed. The repeating issue is alleviated in Fig. A6b.

To summarize, **Config-D** is the best choice for generating short video (less than 10 seconds), while **Config-F** is better for long video generation.

3 EXPERIMENTS

We evaluate our method on several datasets and compare it against prior arts.

Evaluation Metrics. Akin to the literature, Frechet Inception Distance (FID) (Heusel et al., 2017) and Frechet Video Distance (FVD) (Unterthiner et al., 2018) serve as the quantitative metrics to

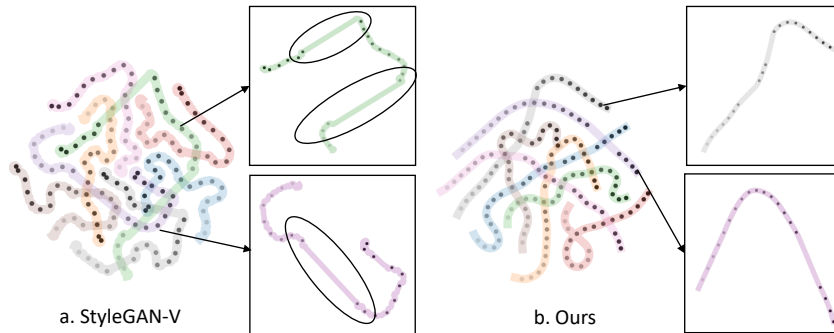


Figure 5: **Visualization of motion embeddings** using T-SNE (Van der Maaten & Hinton, 2008). Each dot refers to a motion code v_t , which represents a single frame’s motion. A set of progressively darkening dots construct one trajectory that represents a synthesized frame sequence. We can tell that there usually exist undesired twists in the motion trajectory of StyleGAN-V (Skorokhodov et al., 2022), indicating the discontinuity of motion embedding. On the contrary, our approach helps alleviate this issue, resulting in smoother transition throughout the entire video.

Table 2: **Quantitative comparison** between our approach and existing video generation methods on SkyTimelapse (Xiong et al., 2018). For all metrics, the smaller number the better.

| Method | FID | FVD ₁₆ | FVD ₁₂₈ |
|---------------------------------------|-------------|-------------------|--------------------|
| MoCoGAN (Tulyakov et al., 2018) | - | 206.6 | 575.9 |
| + StyleGAN2 backbone | - | 85.9 | 272.8 |
| MoCoGAN-HD (Tian et al., 2021) | - | 164.1 | 878.1 |
| VideoGPT (Yan et al., 2021) | - | 222.7 | - |
| DIGAN (Yu et al., 2022) | - | 83.1 | 196.7 |
| LongVideoGAN (Brooks et al., 2022) | - | 116.5 | 152.7 |
| TATS-base (Ge et al., 2022) | - | 132.6 | - |
| StyleGAN-V (Skorokhodov et al., 2022) | 40.8 | 73.9 | 248.3 |
| Ours | 49.9 | 49.0 | 135.9 |

evaluate the synthesis for image and video respectively. In terms of FVD, two temporal spans (consecutive 16 and 128 frames) are chosen to measure the synthesized videos.

Benchmarks. In Sec. 2, we have already conducted comprehensive ablation studies on SkyTimelapse (Xiong et al., 2018), Taichi-HD (Siarohin et al., 2019b), and YouTube Driving dataset (Zhang et al., 2022). To be specific, SkyTimelapse contains over two thousand videos which in average last twenty seconds. Various types of scenes (daytime, nightfall, and aurora) are included. Similar to StyleGAN-V (Skorokhodov et al., 2022), we resize the videos of SkyTimelapse to 256×256 resolution. Taichi-HD contains over three thousand videos recording a person performing Tai-chi. We also resize the videos to 256×256 resolution. YouTube Driving dataset (Zhang et al., 2022) consists of 134 first-view driving videos with a total length of over 120 hours, covering up to 68 cities, showing various conditions, from different weather, different regions, to diverse scene types. The driving scenes have tight geometrical constraints, with most of the objects (vehicles, buildings) following the rigid body constraint. We resize the videos to 180×320 resolution. A part of videos with countryside views in 320×640 resolution is also chosen to benchmark high resolution video generation. For training, we resize them to 256×256 and 512×512 resolution respectively.

Additionally, we compare our approach against previous methods including MoCoGAN (Tulyakov et al., 2018) and its StyleGAN2 based variant, MoCoGAN-HD (Tian et al., 2021), VideoGPT (Yan et al., 2021), DIGAN (Yu et al., 2022), TATS (Ge et al., 2022), LongVideoGAN (Brooks et al., 2022), and StyleGAN-V (Skorokhodov et al., 2022).

Training. We follow the training scheme of StyleGAN-V and train models on a server with 8 A100 GPUs. In terms of various methods and datasets, we grid search the R_1 regularization weight, whose details are available in Appendix. In particular, performances of MoCoGAN and its StyleGAN2 based variant, MoCoGAN-HD, VideoGPT, and DIGAN are directly borrowed from StyleGAN-V paper.

Table 3: **Quantitative comparison** between our approach and existing video generation methods on Taichi-HD (Siarohin et al., 2019b). For all metrics, a smaller number is better.

| Method | FID | FVD ₁₆ | FVD ₁₂₈ |
|---------------------------------------|-------------|-------------------|--------------------|
| MoCoGAN-HD (Tian et al., 2021) | - | 144.7 | - |
| DIGAN (Yu et al., 2022) | - | 128.1 | - |
| TATS-base (Ge et al., 2022) | - | 94.6 | - |
| StyleGAN-V (Skorokhodov et al., 2022) | 33.8 | 152.0 | 267.3 |
| Ours | 26.0 | 84.6 | 176.2 |

Table 4: **Quantitative comparison** between our approach and StyleGAN-V (Skorokhodov et al., 2022) on the self-collected YouTube Driving dataset. For all metrics, a smaller number is better.

| Resolution | Method | FID | FVD ₁₆ | FVD ₁₂₈ |
|------------|------------|-------------|-------------------|--------------------|
| 256 | StyleGAN-V | 28.3 | 449.8 | 460.6 |
| | Ours | 19.2 | 207.2 | 221.5 |
| 512 | StyleGAN-V | 14.6 | 262.4 | 285.4 |
| | Ours | 14.5 | 116.0 | 139.2 |

3.1 MAIN RESULTS

As shown in Tab. 2, our method significantly outperforms existing baselines on SkyTimelapse in terms of FVD₁₆ and FVD₁₂₈. On Taichi-HD, our method achieves consistent improvement in terms of FID, FVD₁₆, and FVD₁₂₈ as reported in Tab. 3. We also compare our method with StyleGAN-V in challenging YouTube Driving dataset. at both 256×256 and 512×512 resolution. For 256×256 resolution in Tab. 4, our method achieves better performance in both FID, FVD₁₆, and FVD₁₂₈. For 512×512 resolution, StyleGAN-V has a comparable FID score but much worse FVD score. For both two resolutions on YouTube driving, we yield a strong performance of less than 50% FVD score than the prior art. As shown in Fig. 1, our method achieves an appealing visual effect, with smooth frame transition.

3.2 STRENGTHS OF THE IMPROVED MODEL

Good translation equivariance. We adopt alias-free technique from image generation for a smooth frame transition. This design also allows for geometric manipulation of the video using a human-specified translation matrix. We showcase several examples in Fig. 6 by feeding different translation matrix to the video generator. It is clear that videos can be successfully translated, and translation equivariance is well maintained over time. This equivariance property improves human controllability over the video generation process.

No jittering phenomenon. As mentioned in Sec. 2.4, discontinuity exists in the motion representation in the prior method, around which jittering phenomenon appears in generated videos. It is caused by linear interpolation between discretized anchor features with fixed interval lengths (256 frames in practice). Our method develops a novel B-Spline based motion representation to ensure the

Table 5: FVD evaluated on the frames around anchors.

| | FVD ₁₆ | FVD ₁₆ -anchor |
|-----------------|-------------------|---------------------------|
| Config-D | 207.2 | 269.1 (+61.9) |
| Config-F | 260.4 | 250.2 (-10.2) |

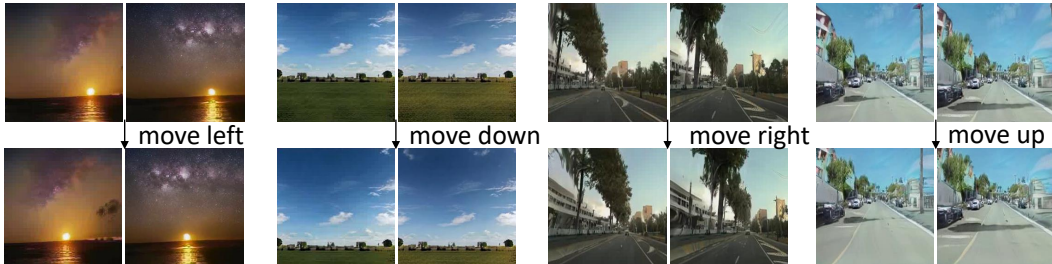


Figure 6: **Application of video 2D translation**, where we are able to control the shift of the frame content, such as moving the setting sun left and moving the grassland down.

temporal smoothness over the anchor features. To quantify the smoothness of generated videos, we sample 16 frames across the anchor (eight frames before and behind the anchor) and calculate the FID_{16} metric (which we name "FID₁₆-anchor") in YouTube Driving dataset. As reported in Tab. 5, **Config-D** suffers from severe performance drop when approaching anchors. While **Config-F** with B-Spline based motion representation maintains the performance, indicating that our method can generate long videos with smooth transitions without performance degrading.

4 RELATED WORK

Unconditional Video generation. Most of the video generation frameworks are built upon GANs (Goodfellow et al., 2014; Brock et al., 2019; Karras et al., 2019; 2020b; 2021; 2018; Radford et al., 2016), owing to their flexibility as well as strong performance in image generation. Prior arts (Tian et al., 2021; Saito et al., 2017; Tulyakov et al., 2018; Fox et al., 2021; Skorokhodov et al., 2022; Yu et al., 2022; Vondrick et al., 2016; Saito et al., 2020; Clark et al., 2019; Wang et al., 2022b) adopt image generators to synthesize frames from a time-coherent sequence of latent codes generated by recurrent networks. To explicitly disentangle the motion from the content, MoCoGAN (Tulyakov et al., 2018) and TGAN (Saito et al., 2017) employ a motion code and a content code as input noise for the generator, serving as a common strategy for the later works. StyleGAN-V (Skorokhodov et al., 2022), which we use as a strong baseline, and DIGAN (Yu et al., 2022) both use implicit neural-based representations for continuous video synthesis. Brooks et al. (2022) leverages a multi-resolution training strategy to prioritize the time axis and ensure long-term consistency. Another line of works (Yan et al., 2021; Kalchbrenner et al., 2017; Weissenborn et al., 2019; Rakhimov et al., 2020; Walker et al., 2021) use autoregressive models to achieve video generation. Kalchbrenner et al. (2017) use a PixelCNN (Van den Oord et al., 2016) decoder to synthesize the next frame pixel by pixel in an autoregressive manner. VideoGPT (Yan et al., 2021) built upon VQ-VAE adopts an autoregressive model to decompose videos into a sequence of tokens. TATS-base (Ge et al., 2022) similarly leverages 3D-VQGAN to decompose videos into tokens and further uses transformers to model the relationship between frame tokens. Additionally, some works using diffusion-based models also present promising results on video generation. Video diffusion (Ho et al., 2022) models entire videos using a 3D video architecture while Yang et al. (2022) uses an image diffusion model to synthesize frames with a recurrent network.

Video generation with guided conditions. A close line of research is video prediction, aiming to generate full videos from the observation of previous frames (Babaeizadeh et al., 2017; Kumar et al., 2019; Lee et al., 2018; Luc et al., 2020; Nash et al., 2022; Finn et al., 2016) or a given conditions (Kim et al., 2020; 2021; Ha & Schmidhuber, 2018). These works typically employ the reconstruction losses to make the future frames predictable for the model. Video translation (Pan et al., 2019; Yang et al., 2018; Wang et al., 2018; Chan et al., 2019; Siarohin et al., 2019a; Ren et al., 2020; Siarohin et al., 2019b) is also a paradigm for video synthesis, which translates the given segmentation masks and keypoints into videos. Some (Li et al., 2022; Liu et al., 2021; Ren & Wang, 2022) focus on synthesizing videos of indoor and outdoor scenes for given camera trajectories, which need to model the 3D scene explicitly. Besides, Ho et al. (2022); Hong et al. (2022); Wu et al. (2021a;b) explore text-to-video generation with diffusion-based models and transformers.

5 CONCLUSION AND DISCUSSION

In this work, we set up a simple yet effective video generation baseline. By introducing the alias-free operations together with pre-learned knowledge, per-frame quality is improved. Explicit temporal modeling in discriminator enhances the dynamic synthesis. In addition, a new B-Spline based motion representation is proposed to enable smooth infinite frame generation. Experimental results show substantial improvements over the previous methods on different datasets.

Discussion. Our approach has several limitations. The current framework follows prior arts using two latent codes to represent content and motion respectively. However, in our experiments, it is suggested that they usually entangle with each other, especially for the driving scenes where it is difficult to separate the content and motion. Moreover, the frame quality is still far from ideal. The object shape is not consistent across consecutive frames, producing apparent artifacts. This could be further improved by introducing structural priors. Last, although we could generate infinite

videos by gradually changing content code, direct control of novel content over time is lacking. [Ge et al. \(2022\)](#) uses explicit planning in the latent space to achieve the controllability of the synthesis, especially for infinite video generation. Similar ideas could be adopted in our framework to improve the quality of long videos.

REFERENCES

- Yuval Alaluf, Or Patashnik, Zongze Wu, Asif Zamir, Eli Shechtman, Dani Lischinski, and Daniel Cohen-Or. Third time’s the charm? image and video editing with stylegan3. *arXiv preprint arXiv:2201.13433*, 2022.
- Mohammad Babaeizadeh, Chelsea Finn, Dumitru Erhan, Roy H Campbell, and Sergey Levine. Stochastic variational video prediction. *arXiv preprint arXiv:1710.11252*, 2017.
- David Bau, Steven Liu, Tongzhou Wang, Jun-Yan Zhu, and Antonio Torralba. Rewriting a deep generative model. In *European conference on computer vision*, pp. 351–369. Springer, 2020.
- Andrew Brock, Jeff Donahue, and Karen Simonyan. Large scale GAN training for high fidelity natural image synthesis. In *Int. Conf. Learn. Represent.*, 2019.
- Tim Brooks, Janne Hellsten, Miika Aittala, Ting-Chun Wang, Timo Aila, Jaakko Lehtinen, Ming-Yu Liu, Alexei A Efros, and Tero Karras. Generating long videos of dynamic scenes. *arXiv preprint arXiv:2206.03429*, 2022.
- Caroline Chan, Shiry Ginosar, Tinghui Zhou, and Alexei A Efros. Everybody dance now. In *Int. Conf. Comput. Vis.*, 2019.
- Aidan Clark, Jeff Donahue, and Karen Simonyan. Adversarial video generation on complex datasets. *arXiv preprint arXiv:1907.06571*, 2019.
- Carl de Boor. Subroutine package for calculating with b-splines. Technical report, Los Alamos National Lab.(LANL), Los Alamos, NM (United States), 1971.
- Chelsea Finn, Ian Goodfellow, and Sergey Levine. Unsupervised learning for physical interaction through video prediction. *Adv. Neural Inform. Process. Syst.*, 2016.
- Gereon Fox, Ayush Tewari, Mohamed Elgharib, and Christian Theobalt. Stylevideogan: A temporal generative model using a pretrained stylegan. *arXiv preprint arXiv:2107.07224*, 2021.
- Songwei Ge, Thomas Hayes, Harry Yang, Xi Yin, Guan Pang, David Jacobs, Jia-Bin Huang, and Devi Parikh. Long video generation with time-agnostic vqgan and time-sensitive transformer. *arXiv preprint arXiv:2204.03638*, 2022.
- Lore Goetschalckx, Alex Andonian, Aude Oliva, and Phillip Isola. Ganalyze: Toward visual definitions of cognitive image properties. In *Int. Conf. Comput. Vis.*, pp. 5744–5753, 2019.
- Ian Goodfellow, Jean Pouget-Abadie, Mehdi Mirza, Bing Xu, David Warde-Farley, Sherjil Ozair, Aaron Courville, and Yoshua Bengio. Generative adversarial nets. In *Adv. Neural Inform. Process. Syst.*, 2014.
- David Ha and Jürgen Schmidhuber. Recurrent world models facilitate policy evolution. In *Adv. Neural Inform. Process. Syst.*, 2018.
- Martin Heusel, Hubert Ramsauer, Thomas Unterthiner, Bernhard Nessler, and Sepp Hochreiter. Gans trained by a two time-scale update rule converge to a local nash equilibrium. *Advances in neural information processing systems*, 30, 2017.
- Jonathan Ho, Tim Salimans, Alexey Gritsenko, William Chan, Mohammad Norouzi, and David J Fleet. Video diffusion models. *arXiv preprint arXiv:2204.03458*, 2022.
- Wenyi Hong, Ming Ding, Wendi Zheng, Xinghan Liu, and Jie Tang. Cogvideo: Large-scale pretraining for text-to-video generation via transformers. *arXiv preprint arXiv:2205.15868*, 2022.

- Ali Jahanian, Lucy Chai, and Phillip Isola. On the "steerability" of generative adversarial networks. *Int. Conf. Learn. Represent.*, 2020.
- Nal Kalchbrenner, Aaron Oord, Karen Simonyan, Ivo Danihelka, Oriol Vinyals, Alex Graves, and Koray Kavukcuoglu. Video pixel networks. In *Int. Conf. Mach. Learn.*, 2017.
- Tero Karras, Timo Aila, Samuli Laine, and Jaakko Lehtinen. Progressive growing of gans for improved quality, stability, and variation. In *Int. Conf. Learn. Represent.*, 2018.
- Tero Karras, Samuli Laine, and Timo Aila. A style-based generator architecture for generative adversarial networks. In *IEEE Conf. Comput. Vis. Pattern Recog.*, 2019.
- Tero Karras, Samuli Laine, Miika Aittala, Janne Hellsten, Jaakko Lehtinen, and Timo Aila. Analyzing and improving the image quality of stylegan. In *Proceedings of the IEEE/CVF conference on computer vision and pattern recognition*, pp. 8110–8119, 2020a.
- Tero Karras, Samuli Laine, Miika Aittala, Janne Hellsten, Jaakko Lehtinen, and Timo Aila. Analyzing and improving the image quality of stylegan. In *IEEE Conf. Comput. Vis. Pattern Recog.*, pp. 8110–8119, 2020b.
- Tero Karras, Miika Aittala, Samuli Laine, Erik Härkönen, Janne Hellsten, Jaakko Lehtinen, and Timo Aila. Alias-free generative adversarial networks. *NIPS*, 34:852–863, 2021.
- Seung Wook Kim, Yuhao Zhou, Jonah Philion, Antonio Torralba, and Sanja Fidler. Learning to Simulate Dynamic Environments with GameGAN. In *IEEE Conf. Comput. Vis. Pattern Recog.*, 2020.
- Seung Wook Kim, , Jonah Philion, Antonio Torralba, and Sanja Fidler. DriveGAN: Towards a Controllable High-Quality Neural Simulation. In *IEEE Conf. Comput. Vis. Pattern Recog.*, 2021.
- Manoj Kumar, Mohammad Babaeizadeh, Dumitru Erhan, Chelsea Finn, Sergey Levine, Laurent Dinh, and Durk Kingma. Videoflow: A conditional flow-based model for stochastic video generation. *arXiv preprint arXiv:1903.01434*, 2019.
- Alex X Lee, Richard Zhang, Frederik Ebert, Pieter Abbeel, Chelsea Finn, and Sergey Levine. Stochastic adversarial video prediction. *arXiv preprint arXiv:1804.01523*, 2018.
- Zhengqi Li, Qianqian Wang, Noah Snavely, and Angjoo Kanazawa. Infinitenature-zero: Learning perpetual view generation of natural scenes from single images. *arXiv preprint arXiv:2207.11148*, 2022.
- Ji Lin, Chuang Gan, and Song Han. Tsm: Temporal shift module for efficient video understanding. In *Int. Conf. Comput. Vis.*, pp. 7083–7093, 2019.
- Andrew Liu, Richard Tucker, Varun Jampani, Ameesh Makadia, Noah Snavely, and Angjoo Kanazawa. Infinite nature: Perpetual view generation of natural scenes from a single image. In *IEEE Conf. Comput. Vis. Pattern Recog.*, 2021.
- Pauline Luc, Aidan Clark, Sander Dieleman, Diego de Las Casas, Yotam Doron, Albin Cassirer, and Karen Simonyan. Transformation-based adversarial video prediction on large-scale data. *arXiv preprint arXiv:2003.04035*, 2020.
- Charlie Nash, João Carreira, Jacob Walker, Iain Barr, Andrew Jaegle, Mateusz Malinowski, and Peter Battaglia. Transframer: Arbitrary frame prediction with generative models. *arXiv preprint arXiv:2203.09494*, 2022.
- Junting Pan, Chengyu Wang, Xu Jia, Jing Shao, Lu Sheng, Junjie Yan, and Xiaogang Wang. Video generation from single semantic label map. In *IEEE Conf. Comput. Vis. Pattern Recog.*, 2019.
- Haonan Qiu, Yuming Jiang, Hang Zhou, Wayne Wu, and Ziwei Liu. Stylefacev: Face video generation via decomposing and recomposing pretrained stylegan3. *arXiv preprint arXiv:2208.07862*, 2022.
- Alec Radford, Luke Metz, and Soumith Chintala. Unsupervised representation learning with deep convolutional generative adversarial networks. In *Int. Conf. Learn. Represent.*, 2016.

- Ruslan Rakhimov, Denis Volkhonskiy, Alexey Artemov, Denis Zorin, and Evgeny Burnaev. Latent video transformer. *arXiv preprint arXiv:2006.10704*, 2020.
- Jian Ren, Menglei Chai, Sergey Tulyakov, Chen Fang, Xiaohui Shen, and Jianchao Yang. Human motion transfer from poses in the wild. In *Eur. Conf. Comput. Vis.*, 2020.
- Xuanchi Ren and Xiaolong Wang. Look outside the room: Synthesizing a consistent long-term 3d scene video from a single image. In *IEEE Conf. Comput. Vis. Pattern Recog.*, 2022.
- Masaki Saito, Eiichi Matsumoto, and Shunta Saito. Temporal generative adversarial nets with singular value clipping. In *Int. Conf. Comput. Vis.*, 2017.
- Masaki Saito, Shunta Saito, Masanori Koyama, and Sosuke Kobayashi. Train sparsely, generate densely: Memory-efficient unsupervised training of high-resolution temporal gan. *Int. J. Comput. Vis.*, 2020.
- Yujun Shen, Ceyuan Yang, Xiaoou Tang, and Bolei Zhou. Interfacegan: Interpreting the disentangled face representation learned by gans. *IEEE Trans. Pattern Anal. Mach. Intell.*, 2020.
- Aliaksandr Siarohin, Stéphane Lathuilière, Sergey Tulyakov, Elisa Ricci, and Nicu Sebe. Animating arbitrary objects via deep motion transfer. In *IEEE Conf. Comput. Vis. Pattern Recog.*, 2019a.
- Aliaksandr Siarohin, Stéphane Lathuilière, Sergey Tulyakov, Elisa Ricci, and Nicu Sebe. First order motion model for image animation. In *Adv. Neural Inform. Process. Syst.*, 2019b.
- Ivan Skorokhodov, Sergey Tulyakov, and Mohamed Elhoseiny. Stylegan-v: A continuous video generator with the price, image quality and perks of stylegan2. In *IEEE Conf. Comput. Vis. Pattern Recog.*, pp. 3626–3636, 2022.
- Yu Tian, Jian Ren, Menglei Chai, Kyle Olszewski, Xi Peng, Dimitris N Metaxas, and Sergey Tulyakov. A good image generator is what you need for high-resolution video synthesis. *Int. Conf. Learn. Represent.*, 2021.
- Sergey Tulyakov, Ming-Yu Liu, Xiaodong Yang, and Jan Kautz. Mocogan: Decomposing motion and content for video generation. In *IEEE Conf. Comput. Vis. Pattern Recog.*, 2018.
- Thomas Unterthiner, Sjoerd van Steenkiste, Karol Kurach, Raphael Marinier, Marcin Michalski, and Sylvain Gelly. Towards accurate generative models of video: A new metric & challenges. *arXiv preprint arXiv:1812.01717*, 2018.
- Aaron Van den Oord, Nal Kalchbrenner, Lasse Espeholt, Oriol Vinyals, Alex Graves, et al. Conditional image generation with pixelcnn decoders. *Adv. Neural Inform. Process. Syst.*, 2016.
- Laurens Van der Maaten and Geoffrey Hinton. Visualizing data using t-sne. *Journal of machine learning research*, 9(11), 2008.
- Carl Vondrick, Hamed Pirsiavash, and Antonio Torralba. Generating videos with scene dynamics. *Adv. Neural Inform. Process. Syst.*, 2016.
- Jacob Walker, Ali Razavi, and Aäron van den Oord. Predicting video with vqvae. *arXiv preprint arXiv:2103.01950*, 2021.
- Sheng-Yu Wang, David Bau, and Jun-Yan Zhu. Rewriting geometric rules of a gan. *ACM Transactions on Graphics (TOG)*, 41(4):1–16, 2022a.
- Ting-Chun Wang, Ming-Yu Liu, Jun-Yan Zhu, Guilin Liu, Andrew Tao, Jan Kautz, and Bryan Catanzaro. Video-to-video synthesis. *arXiv preprint arXiv:1808.06601*, 2018.
- Yaohui Wang, Di Yang, Francois Bremond, and Antitza Dantcheva. Latent image animator: Learning to animate images via latent space navigation. *arXiv preprint arXiv:2203.09043*, 2022b.
- Dirk Weissenborn, Oscar Täckström, and Jakob Uszkoreit. Scaling autoregressive video models. *arXiv preprint arXiv:1906.02634*, 2019.

- Chenfei Wu, Lun Huang, Qianxi Zhang, Binyang Li, Lei Ji, Fan Yang, Guillermo Sapiro, and Nan Duan. Godiva: Generating open-domain videos from natural descriptions. *arXiv preprint arXiv:2104.14806*, 2021a.
- Chenfei Wu, Jian Liang, Lei Ji, Fan Yang, Yuejian Fang, Daxin Jiang, and Nan Duan. N² uva: Visual synthesis pre-training for neural visual world creation. *arXiv preprint arXiv:2111.12417*, 2021b.
- Wei Xiong, Wenhan Luo, Lin Ma, Wei Liu, and Jiebo Luo. Learning to generate time-lapse videos using multi-stage dynamic generative adversarial networks. In *Proceedings of the IEEE Conference on Computer Vision and Pattern Recognition*, pp. 2364–2373, 2018.
- Wilson Yan, Yunzhi Zhang, Pieter Abbeel, and Aravind Srinivas. Videogpt: Video generation using vq-vae and transformers. *arXiv preprint arXiv:2104.10157*, 2021.
- Ceyuan Yang, Zhe Wang, Xinge Zhu, Chen Huang, Jianping Shi, and Dahua Lin. Pose guided human video generation. In *Eur. Conf. Comput. Vis.*, 2018.
- Ceyuan Yang, Yujun Shen, and Bolei Zhou. Semantic hierarchy emerges in deep generative representations for scene synthesis. *Int. J. Comput. Vis.*, 129(5):1451–1466, 2021.
- Ruihan Yang, Prakhar Srivastava, and Stephan Mandt. Diffusion probabilistic modeling for video generation. *arXiv preprint arXiv:2203.09481*, 2022.
- Sihyun Yu, Jihoon Tack, Sangwoo Mo, Hyunsu Kim, Junho Kim, Jung-Woo Ha, and Jinwoo Shin. Generating videos with dynamics-aware implicit generative adversarial networks. *arXiv preprint arXiv:2202.10571*, 2022.
- Qihang Zhang, Zhenghao Peng, and Bolei Zhou. Learning to drive by watching youtube videos: Action-conditioned contrastive policy pretraining. In *European Conference on Computer Vision*, pp. 111–128. Springer, 2022.

APPENDIX

This appendix is organized as follows. appendix A and appendix B present the implementation and dataset details respectively, followed by appendix C and appendix D showing user study result and more visual results.

A IMPLEMENTATION DETAILS.

Our method is developed based on the official implementation of StyleGAN-V (Skorokhodov et al., 2022). We adopt hyper-parameters, the optimizer, the loss function, and the training script to ensure a fair comparison. Notably, the total number of seen images for sufficient data training is 25 million regardless of datasets. We evaluate once after training on every 2.5 million images, and report the result with highest FVD₁₆ score.

Due to statistics variance of different datasets, we search training regularization term, *i.e.* R_1 value, for each method and dataset. Empirically, we find that a smaller R_1 value (*e.g.*, 0.25) works well for pretraining stage (Config-C). While a larger R_1 value (*e.g.*, 4) better suits to video generation learning.

B DATASET DETAILS.

In this section, we introduce the datasets we use, briefly analyze their characteristics and challenges brought for video generation, and show sampled real video frames.

SkyTimelapse. SkyTimelapse (Xiong et al., 2018) is a time-lapse dataset collected from the Internet showing dynamic sky scenes, such as the cloudy sky with moving clouds, and the starry sky with moving stars. It contains various conditions, for instance, different weather conditions (daytime, nightfall, dawn, starry night and aurora), different kinds of foreground object (cloudy sky, starry sky, and sunny sky), and different motion patterns of the sky. It also contains some other objects like trees, mountains, and buildings which further improve the visual diversity. However, since clouds are fluids, there are very few constraints on movement. Minor disturbances and deformations can make a generated video look realistic.

The whole dataset contains over two thousand videos which in average last twenty seconds. We resize the videos to 256×256 following prior works. We sample several video clips in Fig. A1.

YouTube Driving. YouTube Driving Dataset (Zhang et al., 2022) is crawled from YouTube which contains a massive amount of real-world driving frames with various conditions, from different weather, different regions, to diverse scene types. To be specific, 134 videos with a total length of over 120 hours are collected, covering up to 68 cities. Fig. A2 shows sampled frames. The videos are resized to 256×256 resolution for training.

The driving scenes have tighter geometrical constraints, with most of the objects (vehicles, buildings) following the rigid body constraint. The 3D structure of the whole scene should be maintained without any deformation. Besides, different types of objects show different motion patterns. Roads and buildings recede at a reasonable speed opposite to that of ego car, while other cars show lane changes, stops, accelerations.

Countryside. We select a part of videos with countryside scenes from YouTube Driving dataset and resize them to 512×512 resolution for training. We use this dataset to benchmark the performance of generating high-resolution videos. Real samples are presented in Fig. A3.

Taichi-HD. Taichi-HD (Siarohin et al., 2019b) is a collection of YouTube videos recording a single person performing Tai-chi. It contains 3049 training videos in total, with various foreground objects (people with different styles of clothing) and diverse background. It requires realistic human motion generation, which contains non-rigid motion modeling, which poses a significant challenge for video generation.

Table A1: **User study result.** We report the percentage of favorite users for the quality of a set of single images, a set of short videos, and a set of long videos under models from three different settings.

| | YouTube Driving | | | Taichi-HD | | |
|----------|-----------------|----------------|---------------|-----------|----------------|---------------|
| | image(%) | short video(%) | long video(%) | image(%) | short video(%) | long video(%) |
| Config-A | 4 | 6 | 8 | 0 | 2 | 4 |
| Config-D | 62 | 60 | 12 | 52 | 66 | 36 |
| Config-F | 34 | 34 | 80 | 48 | 32 | 60 |

C USER STUDY

To further prove our method’s efficacy, we conduct user study over baseline (**Config-A**), **Config-D**, and **Config-F** on YouTube Driving dataset and Taichi-HD dataset. We evaluate from three perspectives:

Single Image Quality. We provide user with a collection of images randomly sampled from generated videos.

Short Video Quality. We provide user with a collection of generated videos with consecutive 128 frames (up to about 5 seconds).

Long Video Quality. We provide user with a collection of generated videos with consecutive 500 frames (up to 20 seconds).

As shown in Tab. A1, in terms of single image quality, users prefer **Config-D** over other settings in both YouTube Driving and Taichi-HD dataset. The same trend occurs in short video quality assessment. With pre-learned knowledge and a stronger discriminator with temporal shift module (TSM), **Config-D** reaps a significantly higher number of votes. However, for long video generation, **Config-F** becomes the best choice for both YouTube Driving and Taichi-HD dataset. Unnatural jittering and discontinuous motion can drastically affect the users’ video viewing experience. With B-Spline based motion embedding and low rank time modulation, **Config-F** is undoubtedly the best option for long video generation.

D MORE VISUAL RESULTS.

Texture Sticking phenomenon. Texture sticking exists in videos generated by prior methods. Our method leverages the alias-free technique in the generator to overcome this issue. Fig. A4 shows more comparison between our method and StyleGAN-V (Skorokhodov et al., 2022).

Jittering phenomenon. Motion embedding designed in previous method is not first-order continuous, leading to jittering phenomenon when generating long videos. We develop B-Spline based motion embedding which guarantees smoothness and alleviates the problem. We show examples comparing video sequences generated by our method with StyleGAN-V (Skorokhodov et al., 2022) in Fig. A5. Our videos are smooth, without abnormal movements. In videos generated by StyleGAN-V (Skorokhodov et al., 2022), street lights and zebra crossings may suddenly change their moving directions.

Repeating contents. With B-Spline based motion embedding, **Config-E** can compose smooth long videos. However, similar contents appear periodically as shown in Fig. A6a. B-Spline based motion embedding is endowed with so strong capacity that it represents content and motion concepts simultaneously, rather than motion concepts only. We suppress the representation capacity through the low-rank strategy. As shown in Fig. A6b, **Config-F** with low rank time modulation can generate progressively forward contents without repeating contents.

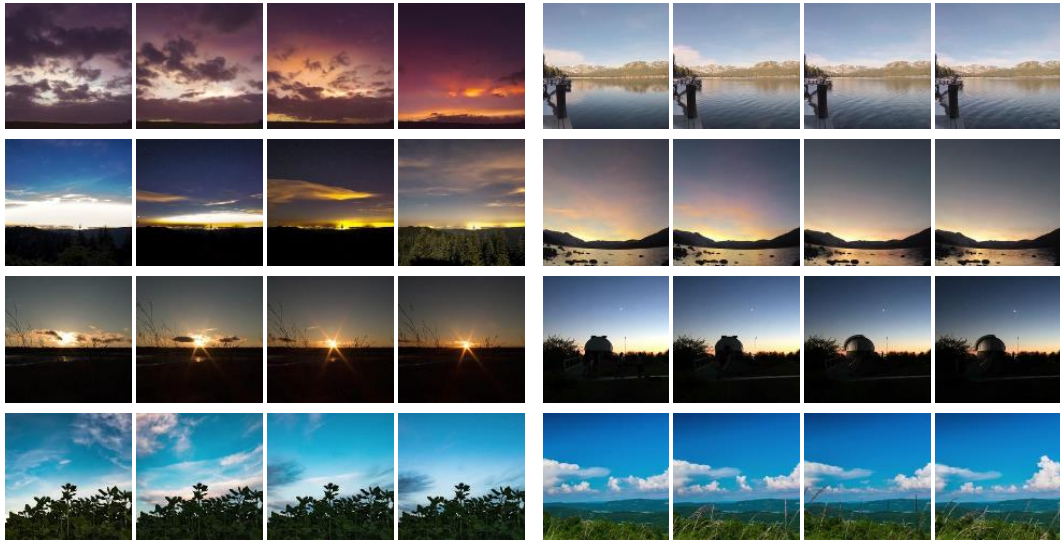


Figure A1: Sampled video frames from SkyTimelapse (Xiong et al., 2018).

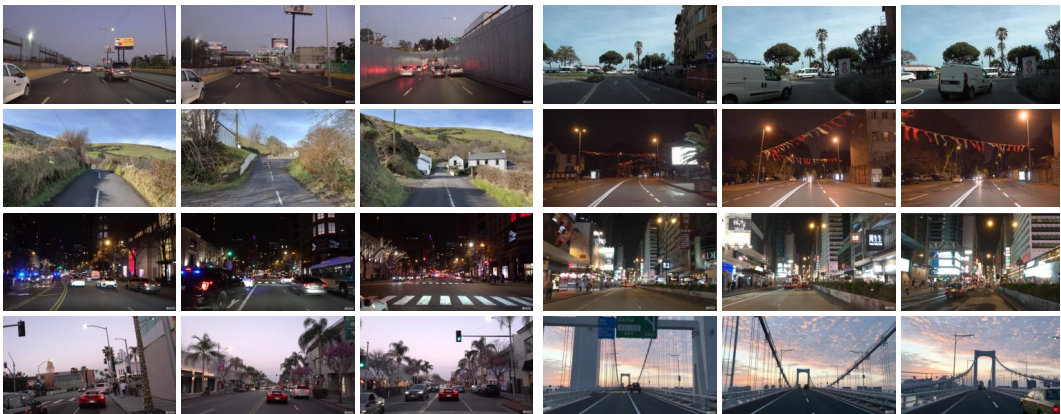


Figure A2: Sampled video frames from YouTube Driving dataset (Zhang et al., 2022).

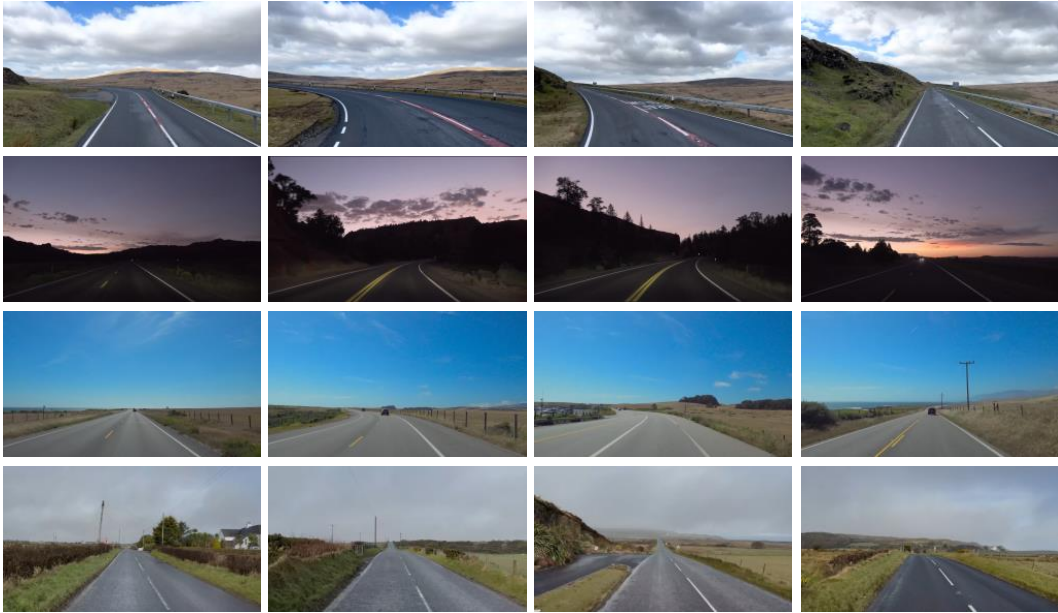


Figure A3: Sampled video frames from Countryside dataset (Zhang et al., 2022).

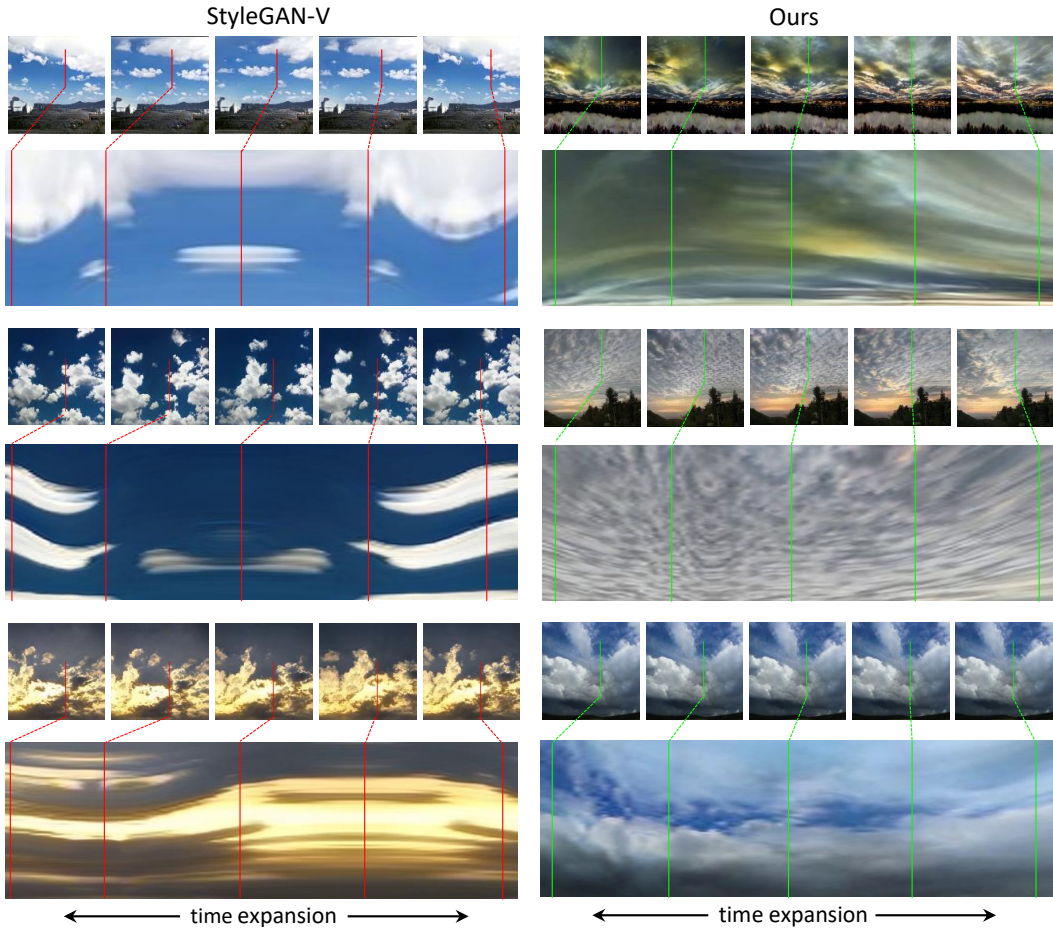


Figure A4: **More examples on texture sticking phenomenon.** We concatenate slices in each frame of the generated video (marked by red and green). We observe *brush effect* when texture sticks at specific location. Instead, our approach achieves more smooth frame transition between neighbor frames.

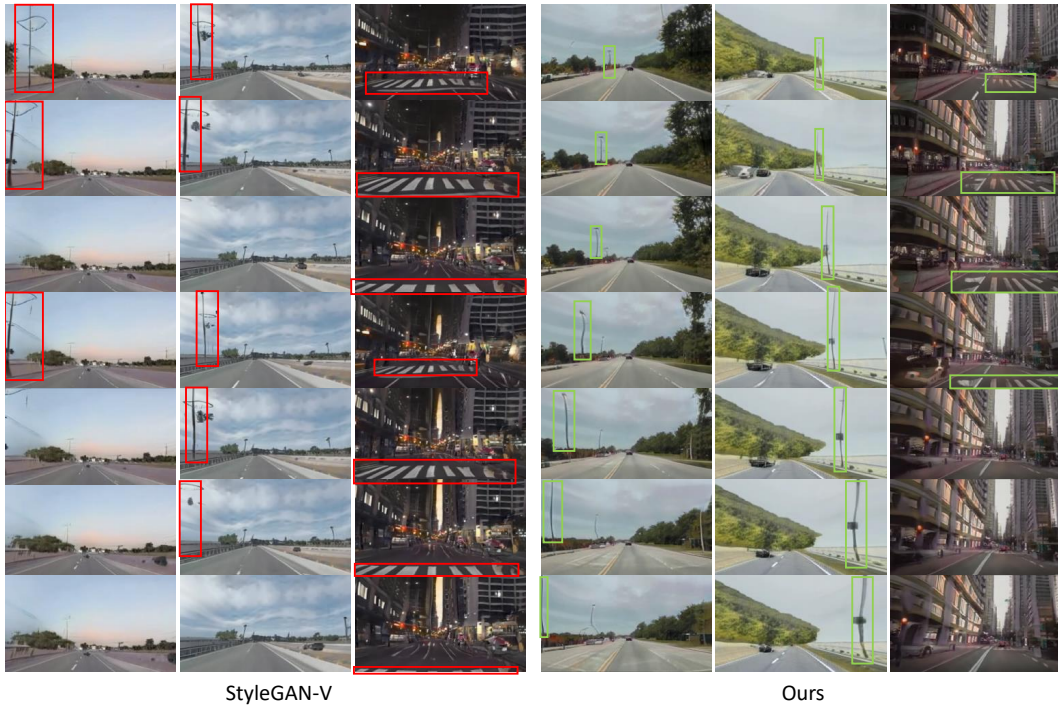


Figure A5: **More examples on jittering phenomenon.** Left three columns denote video frames produced by StyleGAN-V (Skorokhodov et al., 2022). Obviously, as highlighted in red bounding boxes, the street lights and crossroad move unsteadily (*e.g.*, gradually fading out first and suddenly fading in). On the contrary, our approach enables much more reasonable and continuous dynamics of certain objects (see green bounding boxes).

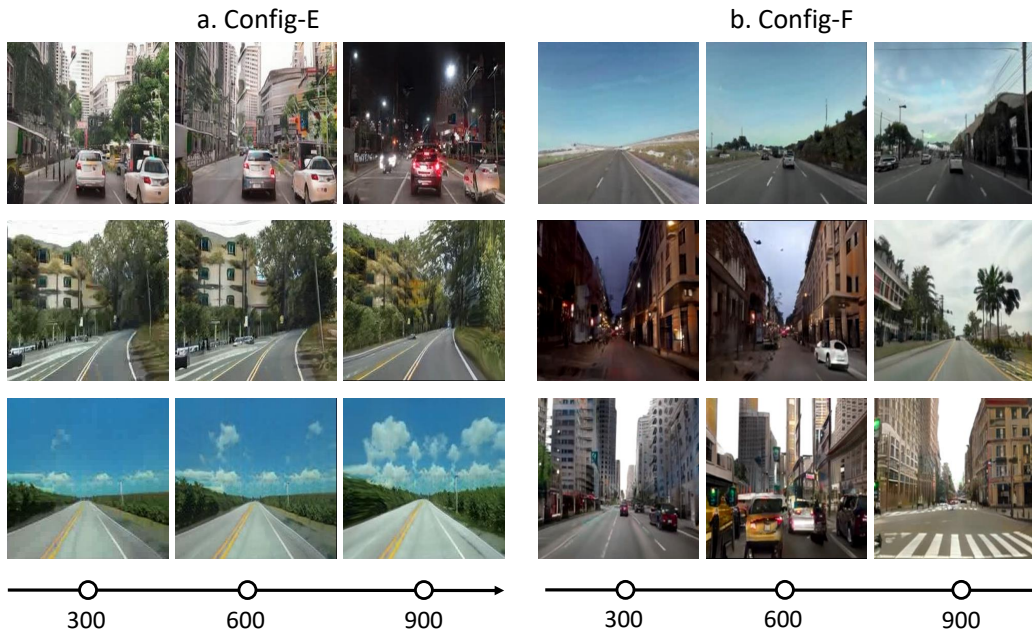


Figure A6: **Examples on repeating contents.** Left three columns denote video frames produced by **Config-E** at the 300th, 600th, and 900th frame respectively. Similar contents (such as foreground objects, and scene layout) periodically appear. In contrast, after adopting low rank time modulation (**Config-F**), contents change gradually without repeating.